



3D printed drug products: Non-destructive dose verification using a rapid point-and-shoot approach



Sarah J Trenfield^a, Alvaro Goyanes^b, Richard Telford^c, David Wilsdon^d, Martin Rowland^e, Simon Gaisford^{a,b}, Abdul W Basit^{a,b,*}

^a UCL School of Pharmacy, University College London, 29-39 Brunswick Square, London WC1N 1AX, UK

^b FabRx Ltd., 3 Romney Road, Ashford, Kent TN24 0RW, UK

^c School of Chemistry and Biosciences, Faculty of Life Sciences, University of Bradford, Bradford BD7 1DP, UK

^d Pfizer Ltd., Analytical Research and Development, Discovery Park, Ramsgate Road, Sandwich CT13 9ND, UK

^e Pfizer Ltd., Drug Product Design, Discovery Park, Ramsgate Road, Sandwich CT13 9ND, UK

ARTICLE INFO

Keywords:

3D printing
Additive manufacturing
Process analytical technology (PAT)
Oral drug delivery systems
Printlets
Digital healthcare

ABSTRACT

Three-dimensional printing (3DP) has the potential to cause a paradigm shift in the manufacture of pharmaceuticals, enabling personalised medicines to be produced on-demand. To facilitate integration into healthcare, non-destructive characterisation techniques are required to ensure final product quality. Here, the use of process analytical technologies (PAT), including near infrared spectroscopy (NIR) and Raman confocal microscopy, were evaluated on paracetamol-loaded 3D printed cylindrical tablets composed of an acrylic polymer (Eudragit L100-55). Using a portable NIR spectrometer, a calibration model was developed, which predicted successfully drug concentration across the range of 4–40% w/w. The model demonstrated excellent linearity ($R^2 = 0.996$) and accuracy (RMSEP = 0.63%) and results were confirmed with conventional HPLC analysis. The model maintained high accuracy for tablets of a different geometry (torus shapes), a different formulation type (oral films) and when the polymer was changed from acrylic to cellulosic (hypromellose, HPMC). Raman confocal microscopy showed a homogenous drug distribution, with paracetamol predominantly present in the amorphous form as a solid dispersion. Overall, this article is the first to report the use of a rapid ‘point-and-shoot’ approach as a non-destructive quality control method, supporting the integration of 3DP for medicine production into clinical practice.

1. Introduction

Three-dimensional printing (3DP) has been forecast to revolutionise the pharmaceutical sector, moving away from a ‘one-size-fits-all’ treatment approach towards personalisation. Indeed, 3DP technology allows medicines to be tailored to the individual needs of each patient, for example, by modifying the dosage, shape, size and release characteristics, as well as via production of multi-drug combinations (Alhnan et al., 2016; Awad et al., 2018a,b; Ghosh et al., 2018; Sadia et al., 2018b; Smith et al., 2018; Trenfield et al., 2018; Verstraete et al., 2018; Zema et al., 2017).

To date, five main 3DP technologies have been researched within pharmaceuticals; binder jet printing (Wang et al., 2006; Yu et al., 2009a,b), fused deposition modelling (FDM) (Gioumouxouzis et al., 2018; Goyanes et al., 2014, 2015a, 2018, 2017a, 2016b; Maroni et al., 2017; Melocchi et al., 2016), semi-solid extrusion (Khaled et al., 2018;

Khaled et al., 2015a,b), selective laser sintering (SLS) (Fina et al., 2018a,b, 2017) and stereolithography (SLA) (Goyanes et al., 2016a; Martinez et al., 2017; Muwaffak et al., 2017; Wang et al., 2016). All of the 3DP technologies follow the 3 D’s of 3D printing (Trenfield et al., 2018); a) design: computer aided design software is used to create the dosage form; b) develop: the selected drug(s) and polymer(s) are blended and loaded into the 3D printer and c) dispense: the 3D dosage form is fabricated, in a layer by layer manner, to meet the design requirements.

Due to the versatile, compact and user-friendly nature of these 3DP processes, it is likely that this technology could initiate a new era of digital pharmacy; with medicine design and production occurring directly at the point of care, such as within hospital and community pharmacies (Awad et al., 2018a; Lim et al., 2018). A proposed treatment pathway could involve clinical data being sent to a clinician for review. A medicine could then be designed to meet the patient’s

* Corresponding author at: UCL School of Pharmacy, University College London, 29-39 Brunswick Square, London WC1N 1AX, UK.
E-mail address: a.basit@ucl.ac.uk (A.W. Basit).

therapeutic requirements (in the form of a digital prescription) and sent to a local 3D printer for dispensing on-demand (Alhnan et al., 2016; Awad et al., 2018a; Trenfield et al., 2018).

Despite the many well-documented benefits that 3DP could provide, adoption of this technology for personalised medicine production has not yet occurred. Indeed, the relative lack of clinical experience, in conjunction with the unique features of 3DP compared with more established manufacturing processes, pose a number of challenges before it can be widely integrated (Norman et al., 2017). Most notably, these relate to the matters of quality control (QC) and safety; such as, how dose verification and drug distribution within the 3D printed tablets can be ensured (Trenfield et al., 2018).

Conventionally, solid oral dosage forms require content uniformity and dose verification testing, typically by using high performance liquid chromatography (HPLC) or UV spectroscopy assays. Such tests are performed on samples from a large batch, which is clearly impossible for a manufacturing process capable of fabricating single tablets. In addition, the tests are destructive, expensive and require highly skilled operators and thus would be impractical within a clinical setting. The best solution would involve utilising a novel, non-destructive tablet characterisation method to permit real-time batch release at the clinic (Trenfield et al., 2018). Process analytical technologies (PAT), such as spectroscopic tools including near infrared (NIR) and Raman spectroscopy, have been previously shown to be capable of monitoring tablet critical quality attributes (CQAs), namely drug content (Meza et al., 2006; Wartewig and Neubert, 2005), hardness (Blanco and Alcalá, 2006; Blanco et al., 2006), drug distribution (Eksi-Kocak et al., 2018; Jérez Rozo et al., 2011) and solid state characteristics (Netchacovitch et al., 2017). In particular, NIR spectroscopy is favourable due to its rapid speed of analysis (seconds), non-invasive and non-destructive nature, ability to analyse solid samples and low cost (Luybaert et al., 2007; Teixeira et al., 2018).

Previous studies have evaluated the use of PAT technologies for drug quantification of two-dimensional (2D) inkjet printed formulations (Edinger et al., 2017; Vakili et al., 2016, 2017). In contrast, to date, no such research has been performed around using a simple, 'point-and-shoot' approach to quantify accurately the dosage within 3D printed drug products. A key benefit of 3DP lies in its ability to flexibly change the dosage form geometry, formulation type or excipients depending on the patient's preferences or therapeutic requirements. Indeed, several papers have reported the differing effects of dosage form shape or structure on both drug release (Fina et al., 2018a; Goyanes et al., 2015c; Martinez et al., 2018; Sadia et al., 2018a; Wang et al., 2016; Yang et al., 2018) and patient acceptability (Goyanes et al., 2017b). As such, a user-friendly and rapid technique that accurately measures dosage irrespective of the formulation design and composition would be highly advantageous.

Therefore, this study aimed to create a model that could predict paracetamol concentration in 3D printed tablets, herein termed printlets, fabricated using SLS. The applicability of the model to tablets of different geometries (cylindrical and torus shapes), as well as those composed of different excipients (acrylic and cellulosic polymers) and different formulation types (oral films) were evaluated. The printlets were also characterised using Raman confocal microscopy to observe drug distribution and solid state characteristics within the printlet structure.

2. Materials and methods

Paracetamol USP grade (Sigma-Aldrich, UK) was used as a model drug (MW 151.16, aqueous solubility at 37 °C: 21.80 g/L) (He et al., 2010). Eudragit L100-55, which is a copolymer of methacrylic acid and ethyl acrylate (1:1 ratio) that dissolves at pH 5.5 and above, was donated by Evonik, UK. Hydroxypropyl methylcellulose (HPMC) Viva-pharm E5 was acquired from JRS PHARMA, Germany. Candurin® Gold Sheen was purchased from Azelis, UK.

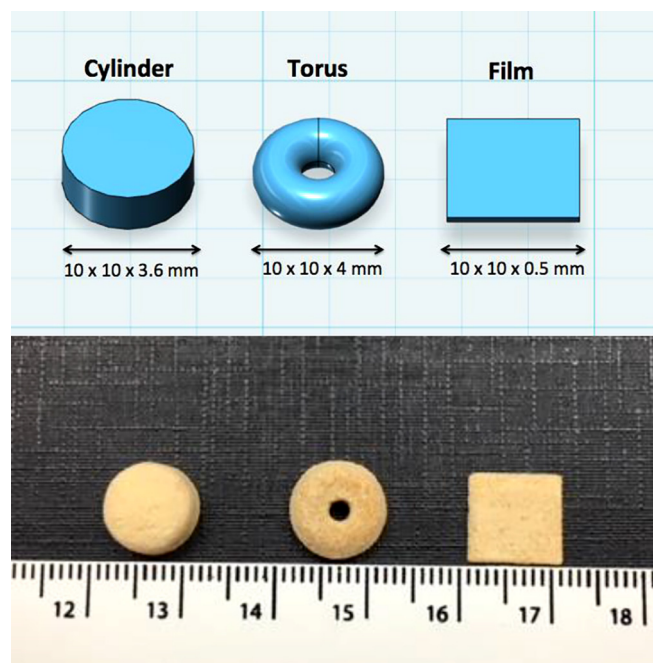


Fig. 1. Printlet designs and printlets of three different geometries; cylinder, torus and film. Ruler units = cm.

2.1. 3D printing process

AutoCAD 2014 (Autodesk Inc., USA) was used to design the templates for the printlets: (cylindrical, 10 mm diameter × 3.6 mm height; torus-shaped, 10 mm diameter × 4 mm height; and oral films, 10 mm × 10 mm × 0.5 mm). Fig. 1 shows examples of each printlet design and image after printing. 3D models were exported as a stereolithography (.stl) file into the 3D printer Sintratec Central software Version 1.1.13.

For all formulations, 70 g of paracetamol and the required excipients were blended using a mortar and pestle (Table 1). 3% w/w of Candurin® Gold Sheen was added to all the formulations to enhance energy absorption from the laser to allow printability. Powder mixtures were transferred to a desktop SLS printer (Sintratec Kit, AG, Brugg, Switzerland) in order to fabricate the printlets. Powder in the reservoir platform (150 mm × 150 mm × 150 mm) of the printer was transferred by a sled to a build platform (150 mm × 150 mm × 150 mm), creating a flat and homogeneously distributed layer of powder.

For all Eudragit L100-55 formulations, the chamber temperature was set to 90 °C, indicating the temperature inside the printer; and the surface temperature was set to 110 °C, indicating the surface temperature of the powder bed during printing. For HPMC E5 formulations,

Table 1

Active and excipient content of printlets (n = 3) used to create NIR calibration model. *Indicates concentrations used for internal validation.

Paracetamol content (% w/w)	Eudragit L100-55 content (%w/w)	Candurin gold sheen content (%w/w)
4	93	3
8	89	3
12*	85	3
16	81	3
20*	77	3
24	73	3
28	69	3
32*	65	3
36	61	3
40	57	3

these temperatures were set at 115 °C and 135 °C, respectively. The printing process started with the activation of a 2.3 W blue diode laser (445 nm; laser scanning speed 100 mm/s) to sinter the powder on to the build platform in a specified pattern based on the .stl file. After the first layer of the printlet had been created, the reservoir platform moved up, the build platform moved down, and the sled distributed a thin layer of powder on top of the powder bed. This process was repeated layer-by-layer until printing was complete. The printlets were then removed from the powder bed and the excess powder was brushed off. Three printlets were printed at the same time for each formulation.

2.2. Near infrared spectroscopy (NIR) data acquisition

NIR reflectance spectra were measured using a portable benchtop Labspec 5000 near infrared spectrometer (Analytical Spectral Devices, USA), equipped with three separate holographic diffraction gratings and three separate detectors; a 512-element silicon photo-diode array for wavelengths between 350–1000 nm, and two TE-cooled InGaAs for wavelengths between 1000–1800 nm and 1800–2500 nm. Spectra were collected using an immobilised lab grade 1 m fibre optic cable (fibre core size 200 µm), which interfaced with the NIR equipment (BIF200-Vis-NIR, Ocean Optics Inc., FL, USA). A Spectralon 99% reflective standard (Labsphere, North Sutton, UK) was used for instrument calibration prior to spectra acquisition. UV–visible-NIR spectra were collected across the 300–2500 nm wavelength region (2200 data points) totalling 64 scans, which were averaged.

Each printlet was analysed at six different points to avoid potential sampling errors and to reduce the variability caused by different surface effects. Standard printlets were scanned twice on the topside, twice on the underside and once on each side. Torus shaped printlets and oral films were scanned three times on the topside and three times on the underside. The final spectrum (used to calculate paracetamol content) was the average of the spectra recorded at the six positions.

2.3. Model development

Seven printlet concentrations ($n = 3$) were selected for calibration model development (4%, 8%, 16%, 24%, 28%, 36% and 40% w/w), and three concentrations ($n = 3$) were used for internal validation (12%, 20% and 32% w/w). Multivariate data analysis was performed using MATLAB software version R2017a (The MathWorks, CA, USA) with the PLS Toolbox version 8.6 (Eigenvector, CA, USA) for data pre-processing and modelling. Partial least squares (PLS) regression was performed on the datasets to build calibration models. The models were internally cross-validated using venetian blinds.

Validation of the NIR calibration model was performed according to International Conference on Harmonization (ICH) guidance Q2(R1) (ICH, 2005), and other regulatory guidance from the European Medicines Agency (EMA) (EMA, 2014) and the Food and Drug Administration (FDA) (FDA, 2015), by assessing model specificity, linearity (expressed as correlation coefficient, R^2), accuracy (expressed as the root mean square error of prediction; RMSEP), precision and intermediate precision (expressed as relative standard deviation; RSD). The predictive performance of the model was evaluated by scanning an external validation set of Eudragit L100-55 printlets at 12%, 20% and 32% w/w concentrations. To evaluate whether the model would work when changing printlet geometry and dosage form type, 3D printed torus shaped printlets and oral films were also scanned. Moreover, the predictive performance of the model in the presence of other excipients was evaluated by changing the polymer to HPMC E5.

2.4. Determination of drug content

Following NIR analysis, each individual printlet was quantitatively analysed for drug content using high performance liquid chromatography (HPLC). Three individual printlets of each formulation were

placed in separate volumetric flasks with deionised water (250 mL). For Eudragit L100-55-based printlets, 3 drops of 5 N NaOH were added to each flask to increase the pH to enable dissolution. Samples of solution were then filtered through 0.22 µm filters (Millipore Ltd., Ireland) and the concentration of drug determined with HPLC (Hewlett Packard 1050 Series HPLC system, Agilent Technologies, UK). The validated HPLC assay entailed injecting 20 µL samples for analysis using a mobile phase, consisting of methanol (15%) and water (85%), through an Ultra C8 5 µm column, 250 × 4.6 mm (Restek, USA) maintained at 40 °C. The mobile phase flow rate was 1 mL min⁻¹ and the eluent was screened at a wavelength of 247 nm.

2.5. Raman spectroscopy and mapping

Raman mapping was performed to evaluate the distribution of drug and polymer within the printlets. The underside surface and cross section of samples (40% w/w) were mounted and focused using a X50 objective on an InVia confocal Raman microscope (Renishaw, UK) equipped with a 300 mW 785 nm HPNIR Renishaw laser. Spectral arrays were acquired with *ca.* 4500 spectra recorded over a *ca.* 300 µm × 300 µm ($X \times Y$) surface of the sample using a step size of 5 µm in X and Y. A 1200 line grating was used providing spectral resolution up to 1 cm⁻¹. Spectra were collected over the range of 1190–1695 nm, with a 2 s exposure time and 2 accumulations.

Processing was performed using Renishaw WiRE software v.3.4 using direct classical least-squares (DCLS) component matching to paracetamol (amorphous and crystalline, form I) and Eudragit L100-55 reference spectra to generate 2-dimensional false colour maps.

2.6. X-ray powder diffraction

X-ray powder diffraction patterns of printlets (ground to a fine powder), formulation blends and pure paracetamol were recorded using a Rigaku MiniFlex 600 (Rigaku, USA) with a Cu K α X-ray source ($\lambda = 1.5418 \text{ \AA}$) and accompanying software Miniflex Guidance version 1.2.01. The intensity and voltage applied were 15 mA and 40 kV. The angular range of data acquisition was 3–40° 2 θ , with a step size of 0.02° at a speed of 2° min⁻¹.

3. Results and discussion

To facilitate the integration of 3DP into pharmacy practice, the development of rapid, non-destructive quality control techniques that permit real time batch release are required. A relatively new 3DP technology to pharmaceuticals is SLS printing which, to date, has been used to manufacture a range of dosage forms, including immediate and controlled release tablets (Fina et al., 2017, 2018a), as well as fast disintegrating oro-dispersible tablets (Fina et al., 2018b). In the present study, for the first time the manufacture of standard cylindrical and novel torus-shaped printlets, as well as 3D printed oral films, containing a high drug loading (up to 40% w/w) were successfully produced (Fig. 1). Paracetamol and Eudragit L100-55 were selected as the model drug and excipient for calibration development.

3.1. Drug distribution and solid state analysis

To ensure paracetamol was homogeneously distributed within the printlets, Raman confocal microscopy was used which is a non-destructive method commonly employed to evaluate drug distribution, as well as the amorphous and crystalline content, of pharmaceutical tablets and films (Goyanes et al., 2015d; Netchacovitch et al., 2017; Scoutaris et al., 2014). Within this study, a 300 µm × 300 µm sized section on the external underside surface and internal cross section of a printlet (40% w/w) was scanned using a Raman microscope. At each point of the formulation mapped, reference paracetamol (amorphous and crystalline; form I) and Eudragit L100-55 spectra were inputted

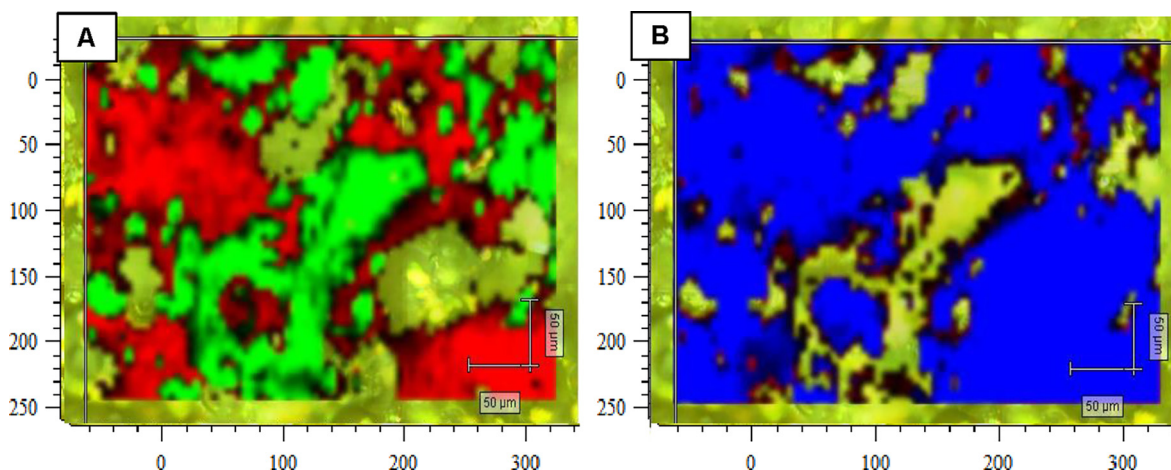


Fig. 2. External underside surface of a printlet (40% w/w paracetamol) mapped using Raman confocal microscopy. Red areas = amorphous paracetamol (A), green areas = crystalline paracetamol (Form I), blue areas = Eudragit L100-55 (B).

into the software and compared with the printlet spectra collected using DCLS.

Paracetamol was homogeneously distributed across the internal structure and surface of the printlet (Fig. 2A and 3A). In particular, the underside surface of the printlet consisted of paracetamol that was mostly present in the amorphous phase (Fig. 2A; red areas). It was found that the distribution of the polymer (Eudragit L100-55) predominantly overlaps with amorphous paracetamol, suggesting that in these areas paracetamol was present as a solid dispersion (Fig. 2B). Similar results have also been reported elsewhere (Fina et al., 2017). There is special interest in delivering drugs as solid dispersions as a strategy to enhance drug dissolution and bioavailability, particularly for drugs with inherently low solubility (e.g. BCS Class II or IV compounds) (Capretto et al., 2017; Martínez et al., 2014). As well as SLS, other thermal 3DP methods have shown the capability of formulating a variety of drugs as amorphous or semi-amorphous systems (Kollamaram et al., 2018; Sadia et al., 2016). Within the SLS printing process, it is likely that the application of heat and laser results in complete drug melting to enable formation of a non-crystalline matrix. This process would differ based on the drug, excipients and printing parameters (e.g. laser scanning speed, chamber temperature) selected.

Areas of crystalline paracetamol form I (green areas) were also present (Fig. 2A). The areas of crystalline material were attributed to the presence of residual unsintered powder on the surface of the tablet that had not been effectively cleared away after printing. To confirm this, a cross section of the same printlet was taken and the internal

structure was viewed using the Raman microscope. Fig. 3A and B show that paracetamol was entirely present in the amorphous phase, which was distributed amongst the Eudragit L100-55 matrix as a solid dispersion. This confirms that the amorphous material was not re-crystallising out of the matrix and is instead likely due to remaining unsintered powder on the surface. Excess powder remaining on the surface or trapped inside the pores of the SLS printed objects has previously been reported (Bose et al., 2013; Williams et al., 2005).

To verify the Raman microscopy findings, XRPD data were collected for both the powder blends and the standard printlets (Fig. 4). For the 20% and 40% w/w drug-loaded powder blends, characteristic paracetamol form I peaks can be observed although these were not observed at the 4% concentration. It is likely that, while paracetamol would be present in the crystalline form at 4% w/w, it would be below the detection limit of XRPD analysis. For the printed formulations, the 20% w/w concentration showed complete conversion of paracetamol into the amorphous form, confirming that the drug was dispersed into the polymer matrix. At 40% w/w, it can be seen that the majority of paracetamol has been converted into the amorphous form (due to peak height reduction), although several crystalline paracetamol peaks can be observed. This is most likely attributed to the presence of residual unsintered powder on the surface of the printlet, which was observed in the aforementioned Raman maps (Figs. 2 and 3).

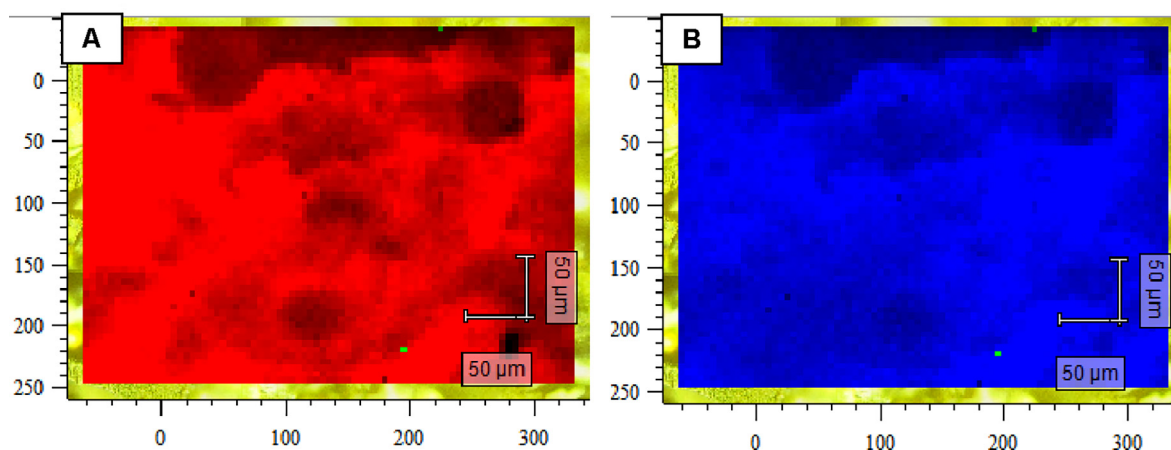


Fig. 3. Internal cross section of a printlet (40% w/w paracetamol) mapped using Raman confocal microscopy. Red areas = amorphous paracetamol (A), blue areas = Eudragit L100-55 (B).

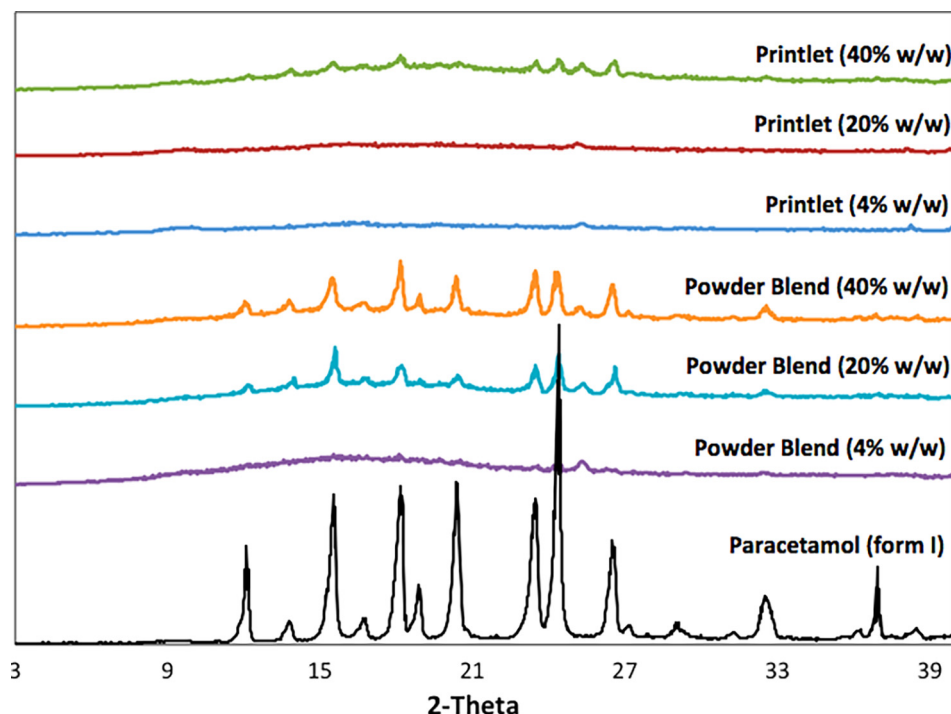


Fig. 4. X-ray powder diffraction patterns of pure paracetamol (form I), powder blends (4%, 20% and 40% w/w paracetamol) and printlets (4%, 20% and 40% w/w paracetamol).

3.2. Quantitative analysis using NIR

To create a reliable multivariate calibration model, the evaluation of different spectral pre-processing methods was required in order to extract the relevant chemical information. In this study, a total of ten PLS models were developed (Table 2); six different pre-treatments were applied to the spectra and for each, two different spectral ranges were evaluated; SR1: 1100–2360 nm and SR2: 1300–2100 nm. For each model, the correlation coefficient of the calibration curve (R^2 Cal) and the standard error of the calibration curve (RMSEC) were calculated in order to determine the predictive performance of the model. The correlation coefficient of the test printlets (R^2 Pred) and standard error of the test printlets (RMSEP) were then calculated for the validation set and the most suitable model was defined as the model with the lowest RMSEP value with high linearity (i.e. R^2 Pred as close to 1 as possible). In this case, the model selected was model 10, which covered the 1300–2100 nm wavelength range with a 2nd derivative (Savitzky-Golay method: filter width of 41 with a 2nd polynomial (Savitzky and Golay, 1964)) and mean-centering pre-processing technique. These pre-treatments are commonly used to improve the accuracy of quantification by enhancing spectral information, reducing baseline drift and reducing

error caused by light scattering effects (Chalus et al., 2005).

The calibration model developed covered a total of 30 samples (with 7 concentrations being selected for calibration and 3 for validation) over a paracetamol concentration range of 4–40% w/w. Fig. 5 shows the developed calibration model showing the correlation between NIR predicted values and the reference concentrations determined with HPLC. Favourably, the model demonstrated excellent linearity ($R^2 = 0.996$), confirming that the NIR test results were proportional to paracetamol concentration in the stated range.

In addition to linearity, further validation of the model was performed by determining several parameters (recommended by ICH (ICH, 2005), FDA (FDA, 2015) and EMA (EMA, 2014) guidelines). These included model specificity, accuracy, precision and intermediate precision.

3.2.1. Specificity

For the model to be fit-for-purpose, it must have the ability to identify explicitly the analyte (i.e. paracetamol) in the presence of the other components (i.e. Eudragit L100-55 and the colourant). This was evaluated by comparing the loadings spectra of the 1st latent variable (LV1), which accounted for 88.8% of the variation in the data, to the

Table 2

Comparison of different spectral pre-processing methods and spectral wavelength ranges to develop calibration model. SNV: Standard Normal Variant, D₂: Second derivative spectra (Savitzky-Golay method), MSC: Multiplicative Scatter Correction.

Wavelengths (nm)	Model Code	Data pre-treatments	Latent Variables	R^2 (Cal)	RMSEC (%)	R^2 (Pred)	RMSEP (%)
1100–2360	1	None	2	0.974	2.05	0.956	2.45
	2	SNV	2	0.992	1.15	0.985	1.11
	3	MSC	3	0.992	1.16	0.985	1.10
	4	MSC + D ₂	2	0.985	1.54	0.957	2.25
	5	D ₂	2	0.990	1.30	0.987	1.25
1300–2100	6	None	3	0.995	0.95	0.990	0.82
	7	SNV	2	0.991	1.23	0.969	1.53
	8	MSC	2	0.991	1.24	0.970	1.50
	9	MSC + D ₂	2	0.990	1.27	0.986	1.16
	10	D ₂	3	0.996	0.83	0.995	0.63

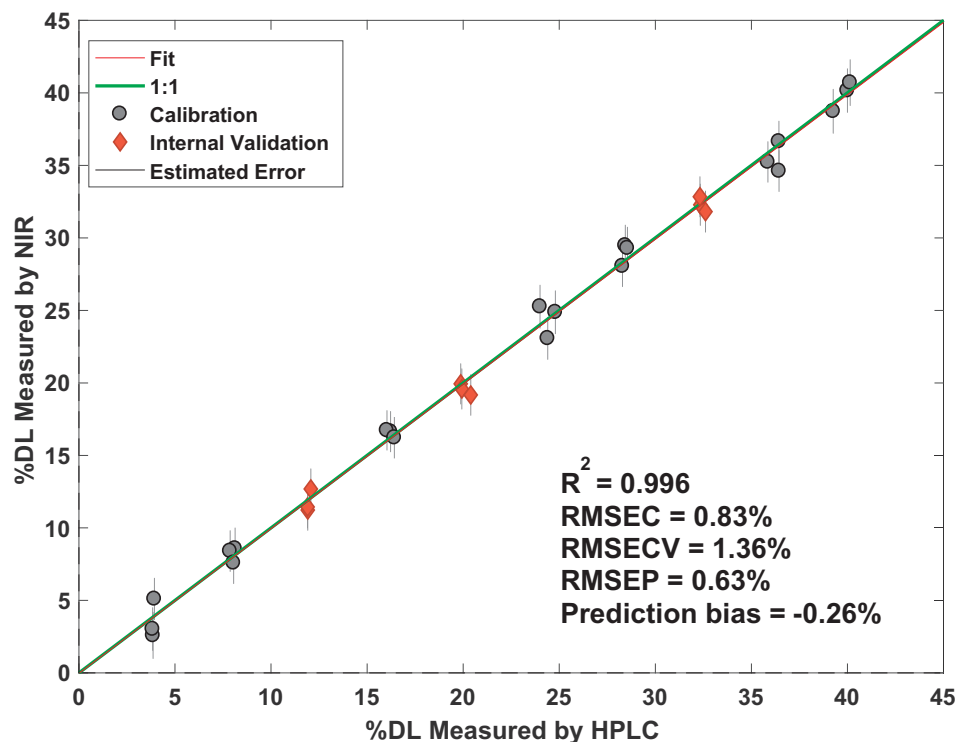


Fig. 5. PLS model of NIR predicted vs. HPLC determined paracetamol content (%drug load; %DL) of printlets. Grey points are calibration (7 concentrations), red points are validation (3 concentrations).

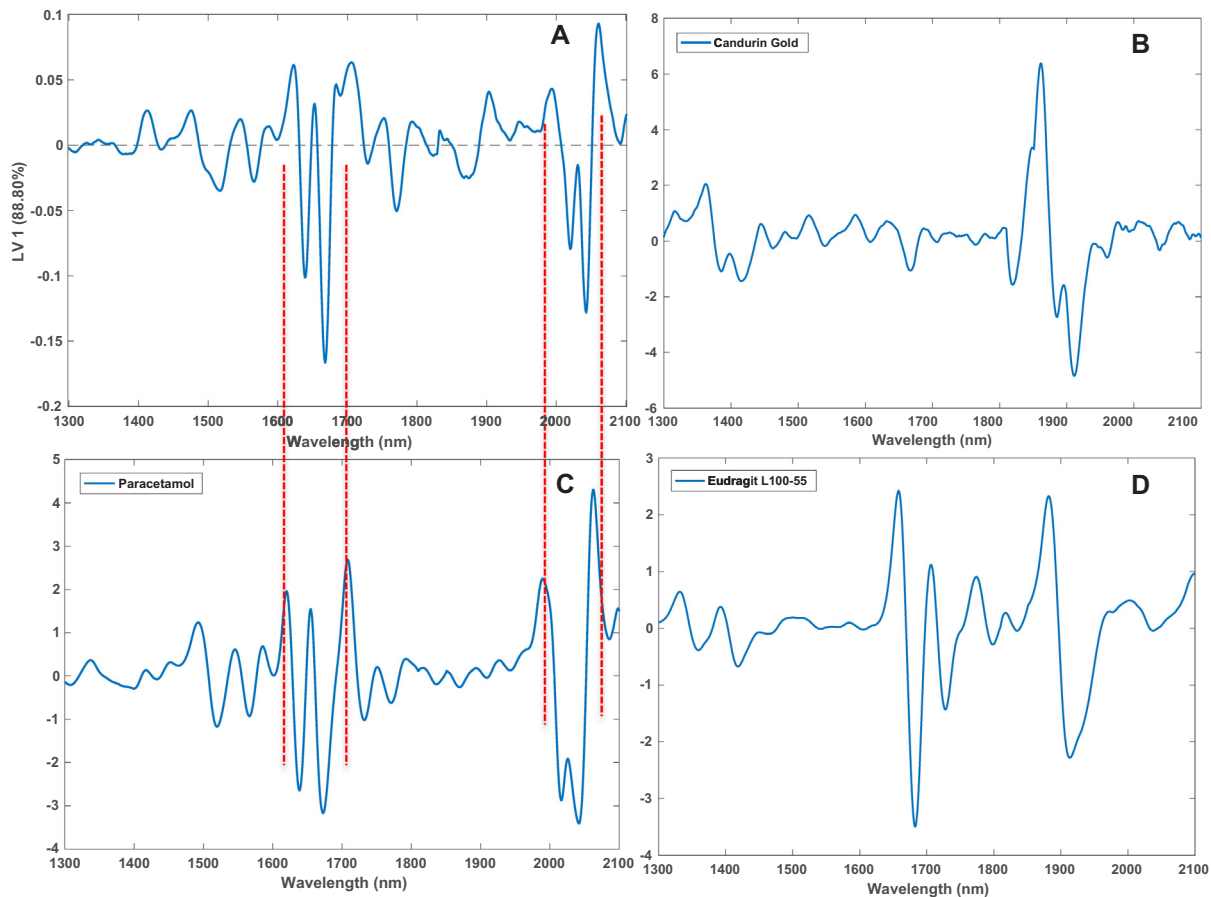


Fig. 6. The 2nd derivative spectra of: A) PLS LV1 loading spectra; B) reference paracetamol; C) reference Eudragit L100-55; D) reference Candurin Gold Sheen. Red dashed lines highlight the presence of similar spectral features.

Table 3

Results of dose predicted using the NIR model vs. the reference HPLC method. Target concentrations; A: 12% w/w, B: 20% w/w, C: 32% w/w.

Tablet	Test Validation Set					
	A (% w/w)		B (% w/w)		C (% w/w)	
	HPLC	NIR	HPLC	NIR	HPLC	NIR
1	11.89	11.30	20.38	19.15	32.34	32.94
2	12.07	12.70	19.86	20.15	32.31	32.37
3	11.90	11.19	19.93	19.77	32.61	32.03
Mean ± SD	11.95 ± 0.10	11.73 ± 0.84	20.05 ± 0.28	19.69 ± 0.50	32.42 ± 0.17	32.44 ± 0.46
P value	0.65 (NS)		0.50 (NS)		0.94 (NS)	

reference component spectrum in the 2nd derivative (Fig. 6A and C). LV1 was found to model well-known paracetamol spectral features at 1625–1675 nm (Trafford et al., 1999) and 2000–2050 nm (highlighted by the red dashed lines on Fig. 6). LV1 was not found to be modelling the common spectral features of Eudragit L100-55 or Candurin Gold Sheen (Fig. 6B and 6D). This confirmed that the majority of the variation in the data was caused by the change in paracetamol concentration. Un-processed and pre-processed spectra of both the raw materials and the scanned printlets (4–40% w/w) have been provided in Supplementary files Figs. 1 and 2.

Supplementary data associated with this article can be found, in the online version, at <https://doi.org/10.1016/j.ijpharm.2018.08.002>.

3.2.2. Accuracy

The accuracy of the calibration model can be expressed as the closeness in agreement between the reference HPLC and the predicted NIR values (Table 3). ICH Q2 guidance recommends assessing accuracy using a minimum of nine determinations over a minimum of three concentration levels (ICH, 2005). As such, standard printlets (n = 3) from three concentration levels (A: 12%, B: 20% and C: 32% w/w) were scanned. Table 3 shows the difference between the HPLC and NIR predicted paracetamol concentrations. Paired *t*-test results showed that there were no significant differences between the HPLC and NIR methods ($p > 0.05$) across all three concentrations, confirming that NIR is a suitable quantification method for standard printlets. Compared with HPLC, NIR predictions displayed a slightly higher SD, which was more evident at lower concentrations. This is likely due to minute differences in the surface effects of the printlets. However, this was not

as high for the generally allowed limits of 85–115% required for content uniformity testing by the MHRA (MHRA, 2018). Accuracy was also confirmed by having a low error value (RMSEP of 0.63%) and low prediction bias of -0.26% , which were similar to findings in the literature (Trafford et al., 1999) (Fig. 5).

One of the main benefits of 3D printing for personalised medicine is the ability to tailor solid dosage form shape and size, depending on the patient preference or therapeutic needs (Trenfield et al., 2018). Several studies have already shown that changing printlet geometry can alter the dose and drug release characteristics (Goyanes et al., 2015c; Martinez et al., 2018; Sadia et al., 2018a). It is also well known that NIR absorbance can be affected by tablet surface effects (Jamrógiewicz, 2012; Saeed et al., 2009) and, as such, it was important to evaluate the performance of the developed PLS model when scanning printlets of different geometries.

To determine this, torus shaped printlets (12%, 20% and 32% w/w) and oral films with the same formulation composition as the standard shape were scanned at six different points on the formulation. Fig. 7A and B show that the model predicted the concentrations well, as the points fitted on the calibration curve. Torus shaped printlets displayed a slightly higher error compared to oral films (RMSEP values of 2.05% and 1.14%, respectively), which is likely due to the complex rounded surface structure of this shape, compared with the flat films. However, overall the model continued to be fit-for-purpose for use with differently shaped tablets of the same composition.

A further benefit of using 3DP for personalised medicine is the flexibility of changing excipients based on the intended drug release characteristics. Previous studies have highlighted the effects of different

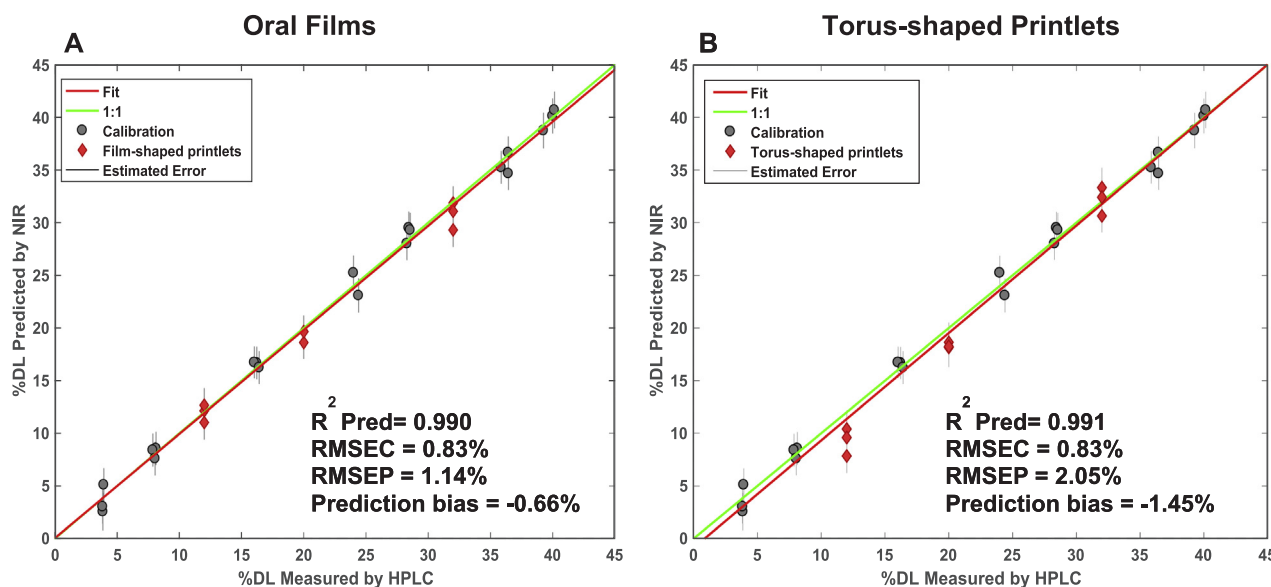


Fig. 7. PLS models of NIR predicted vs. HPLC determined paracetamol content (% drug load; %DL) of A) film shaped printlets and B) torus shaped printlets. Grey points are calibration (7 concentrations), red points are the test sets (3 concentrations).

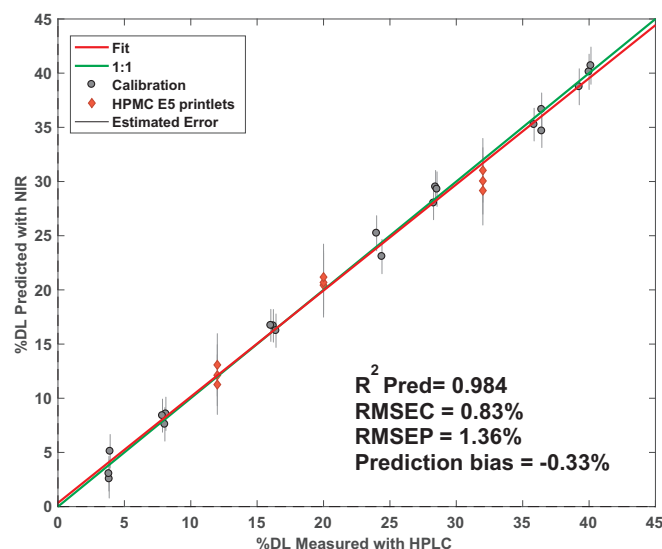


Fig. 8. PLS model of NIR predicted vs. HPLC determined paracetamol content (%drug load; %DL) of standard shaped HPMC E5 printlets. Grey points are calibration (7 concentrations composed of Eudragit L100-55), red points are the test sets (3 concentrations composed of HPMC E5).

polymer types (Ehtezazi et al., 2018; Fina et al., 2018a; Goyanes et al., 2015b; Kadry et al., 2018; Kempin et al., 2017; Zhang et al., 2017) and grades (Goyanes et al., 2017a) on drug dissolution. In the present study, the calibration model was developed using an acrylate-based polymer (Eudragit L100-55), however the ability for this model to be applied to another type of polymer was evaluated. In particular, an external test set of cylindrical printlets were printed that were composed of HPMC E5, an immediate release cellulosic polymer, and the predictive performance of the model was evaluated (Fig. 8).

Despite the change in polymer, an excellent predictive performance was observed (high linearity; $R^2 = 0.984$, high accuracy; RMSEP = 1.36%; Fig. 8). Generally, changing the formulation composition can have varying effects on the model prediction. In this case, Q residuals and Hotelling T^2 scores (Fig. 9) were evaluated which are statistical tests that can provide a quantitative assessment of anomalous samples (Li et al., 2010). Both the Q residuals and T^2 scores were high and well exceeded the pre-determined 95% confidence levels,

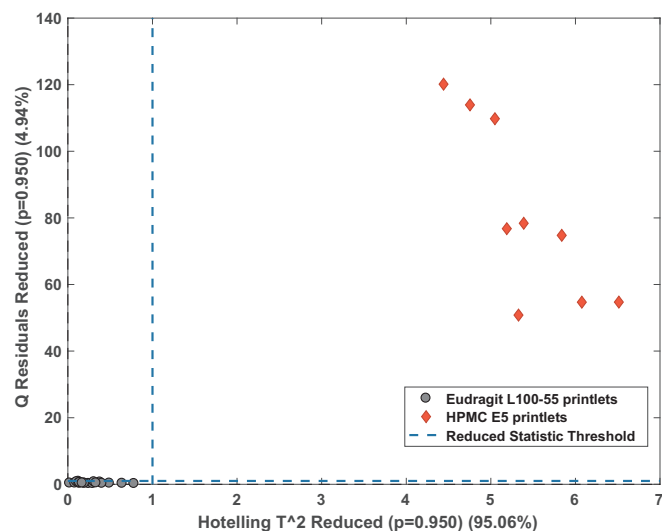


Fig. 9. Q residuals vs. Hotelling T^2 plot. Grey points = calibration printlets (composed of Eudragit L100-55); red points = test printlets (composed of HPMC E5).

indicating that the test printlets were not similar to the calibration printlets and could hence be deemed as ‘outliers’. Despite this, the model maintained a good predictive performance which is likely due to the majority of the data variation being attributed to the change in paracetamol concentration (LV1 = 88.8%) rather than the polymer. However, from a regulatory perspective and to ensure model accuracy in the clinic, it is likely that a calibration model that covers the expected excipient changes or, alternatively, a separate model for different printlet compositions would have to be devised.

3.2.3. Precision

The precision of the calibration model required evaluation to elucidate the degree of agreement between separate test results upon repeated sampling. In the present study, precision was evaluated by scanning a low dose printlet (6% w/w), in triplicate on each of the six points, at the same time of day whilst using the same equipment. Six different points were scanned and averaged for each tablet to reduce the potential spectral variability caused by differing surface effects. However, this number could be reduced further, for example, by using larger probes that could scan a bigger region of the tablet surface.

If a 3D printer were to be integrated into pharmacy practice, it is likely that printlets would be produced at different times of day and in different locations. As such, intermediate precision was also evaluated by performing the same test two weeks later, at a different time of day and in a different equipment location. Table 4 shows the results of precision and intermediate precision. For both tests, the standard deviation was low (0.06 and 0.23% w/w, respectively) and was below the RMSEP value of 0.63%, again demonstrating model accuracy. For precision and intermediate precision, the relative standard deviation (RSD) values were also low at < 5% (0.91% and 3.80%, respectively), demonstrating that the model displays good precision in different experimental conditions. Compared with HPLC, the use of NIR to measure drug concentration demonstrated a higher SD and RSD, which is not unexpected due to the known impact of surface effects on NIR spectra. However, as an alternative method to measure drug concentration in the clinic, the error demonstrated is low and would be unlikely to be of clinical significance.

Validation of the developed PLS model confirmed that the use of NIR spectroscopy could provide a feasible alternative to conventional, destructive dose verification methods (e.g. HPLC and UV spectroscopy). Favourably, the ‘point-and-shoot’ approach developed in the present study is highly user-friendly and provides a rapid dose prediction with each tablet scan lasting only ~10 s. As such, it is likely that the developed model would be suitable for QC purposes in the clinic. Previous research has mainly focussed on demonstrating this concept for inkjet printed pharmaceuticals. For example, Vakili et al. developed a colourimetric quantification technique for oral films by adding a colourant to the drug-loaded ink which was scanned using a colourimeter (Vakili et al., 2016). By increasing the number of layers printed, a greater intensity of colour was detected and, as such, the dose could be quantified. The same research group also demonstrated the feasibility of using of a handheld NIR spectrometer to predict levothyroxine and prednisolone content in inkjet printed oro-dispersible films (Vakili et al., 2017).

Table 4

Results of precision and intermediate precision experiments using the NIR model vs. the reference HPLC method.

Scan	Precision (%DL)	Intermediate Precision (%DL)	HPLC results (%DL)
1	6.01	5.67	5.84
2	6.11	6.02	5.82
3	6.02	6.09	5.80
Mean \pm SD (%)	6.05 \pm 0.06	5.93 \pm 0.23	5.82 \pm 0.02
RSD (%)	0.91	3.80	0.34

The use of NIR chemical imaging (NIR-CI) as a quality control method for hot melt extruded filaments and printlets has also been evaluated (Khorasani et al., 2016). The researchers used multivariate curve resolution-alternative least squares (MCR-ALS) to predict drug content. However, in that study a calibration model was not used and, as such, MCR-ALS could only be classed as a semi-quantitative method. For a full quantitative characterisation, the development of a calibration model using partial least squares (PLS) regression is widely used (Ravn et al., 2008; Roggo et al., 2007) with the FDA and EMA guidance recognising the use of PLS as a quantitative tool (EMA, 2014; FDA, 2015). As such, it is likely that the developed model in the present study would be more suitable for QC purposes in the clinic.

Due to the development of small spectroscopic systems, in the future, these platforms could be integrated within a 3D printer. This advancement could overcome the regulatory challenges surrounding the integration of 3D printing in clinical practice by providing the ability to both personalise dosage forms and ensure QC within a single step process.

4. Conclusion

3DP is forecast to transition the manufacture of medicines away from a 'one-size-fits-all' approach towards personalisation. To facilitate integration of 3DP into clinical pharmacy practice, the evaluation of non-destructive dose verification and characterisation techniques are required to ensure final product quality. This article has demonstrated the feasibility of using process analytical technologies to measure paracetamol concentration (4–40% w/w) in printlets of different geometries, formulation types and excipients. The developed model was validated according to current international standards, demonstrating excellent linearity ($R^2 = 0.996$) and accuracy (RMSEP = 0.63%). This manuscript reports for the first time the development of a rapid, non-destructive quality control method for 3D printed dosage forms, providing a transformative approach to support the integration of 3DP into clinical pharmacy practice.

Acknowledgements

The authors would like to thank Dr. Mark Underhill and Dr. Katherine Curran for the use of the Labspec 5000 NIR spectrometer. The authors thank the Engineering and Physical Sciences Research Council, United Kingdom (EPSRC), UK for their financial support (EP/L01646X).

References

Alhnan, M.A., Okwuosa, T.C., Sadia, M., Wan, K.W., Ahmed, W., Arafat, B., 2016. Emergence of 3D printed dosage forms: opportunities and challenges. *Pharm. Res.* 33, 1817–1832.

Awad, A., Trenfield, S.J., Gaisford, S., Basit, A.W., 2018a. 3D printed medicines: a new branch of digital healthcare. *Int. J. Pharm.* 548, 586–596.

Awad, A., Trenfield, S.J., Goyanes, A., Gaisford, S., Basit, A.W., 2018b. Reshaping drug development using 3D printing. *Drug Discovery Today*. <https://doi.org/10.1016/j.drudis.2018.05.025>.

Blanco, M., Alcalá, M., 2006. Content uniformity and tablet hardness testing of intact pharmaceutical tablets by near infrared spectroscopy: a contribution to process analytical technologies. *Anal. Chim. Acta* 557, 353–359.

Blanco, M., Alcalá, M., González, J.M., Torras, E., 2006. A process analytical technology approach based on near infrared spectroscopy: tablet hardness, content uniformity, and dissolution test measurements of intact tablets. *J. Pharm. Sci.* 95, 2137–2144.

Bose, S., Vahabzadeh, S., Bandyopadhyay, A., 2013. Bone tissue engineering using 3D printing. *Mater. Today* 16, 496–504.

Li, B., Ryan, P.W., Ray, B.H., Leister, K.J., Sirimuthu, N.M., Ryder, A.G., 2010. Rapid characterization and quality control of complex cell culture media solutions using Raman spectroscopy and chemometrics. *Biotechnol. Bioeng.* 107, 290–301.

Capretto, L., Byrne, G., Trenfield, S.J., Dowden, L., Booth, S., 2017. Oral Formulation Roadmap from Early Drug Discovery to Development. Chapter 7: Formulation, Analytical, and Regulatory Strategies for First-in-Human Clinical Trials. John Wiley & Sons Inc, USA.

Chalus, P., Roggo, Y., Walter, S., Ulmschneider, M., 2005. Near-infrared determination of active substance content in intact low-dosage tablets. *Talanta* 66, 1294–1302.

Edinger, M., Bar-Shalom, D., Rantanen, J., Genina, N., 2017. Visualization and non-destructive quantification of inkjet-printed pharmaceuticals on different substrates

using Raman spectroscopy and Raman chemical imaging. *Pharm. Res.* 34, 1023–1036.

Ehtezazi, T., Algellay, M., Islam, Y., Roberts, M., Dempster, N.M., Sarker, S.D., 2018. The application of 3D printing in the formulation of multilayered fast dissolving oral films. *J. Pharm. Sci.* 107, 1076–1085.

Eksi-Kocak, H., Ilbasmis Tamer, S., Yilmaz, S., Eryilmaz, M., Boyaci, I.H., Tamer, U., 2018. Quantification and spatial distribution of salicylic acid in film tablets using FT-Raman mapping with multivariate curve resolution. *Asian J. Pharm. Sci.* 13, 155–162.

EMA, 2014. Guideline on the use of near infrared spectroscopy by the pharmaceutical industry and the data requirements for new submissions and variations.

FDA, 2015. Development and Submission of Near Infrared Analytical Procedures. Guidance for Industry.

Fina, F., Goyanes, A., Gaisford, S., Basit, A.W., 2017. Selective laser sintering (SLS) 3D printing of medicines. *Int. J. Pharm.* 529, 285–293.

Fina, F., Goyanes, A., Madla, C.M., Awad, A., Trenfield, S.J., Kuek, J.M., Patel, P., Gaisford, S., Basit, A.W., 2018a. 3D printing of drug-loaded Gyroid lattices using selective laser sintering. *Int. J. Pharm.* 547, 44–52.

Fina, F., Madla, C.M., Goyanes, A., Zhang, J., Gaisford, S., Basit, A.W., 2018b. Fabricating 3D printed orally disintegrating printlets using selective laser sintering. *Int. J. Pharm.* 541, 101–107.

Ghosh, U., Ning, S., Wang, Y., Kong, Y.L., 2018. Addressing unmet clinical needs with 3D printing technologies. *Adv. Healthcare Mater.* <https://doi.org/10.1002/adhm.201800417>.

Gioumouxouzis, C.I., Baklavardis, A., Katsamenis, O.L., Markopoulou, C.K., Bouropoulos, N., Tzetzis, D., Fatouros, D.G., 2018. A 3D printed bilayer oral solid dosage form combining metformin for prolonged and glimepiride for immediate drug delivery. *Eur. J. Pharm. Sci.* 120, 40–52.

Goyanes, A., Buanz, A.B.M., Basit, A.W., Gaisford, S., 2014. Fused-filament 3D printing (3DP) for fabrication of tablets. *Int. J. Pharm.* 476, 88–92.

Goyanes, A., Buanz, A.B.M., Hatton, G.B., Gaisford, S., Basit, A.W., 2015a. 3D printing of modified-release aminosaliclylate (4-ASA and 5-ASA) tablets. *Eur. J. Pharm. Biopharm.* 89, 157–162.

Goyanes, A., Chang, H., Sedough, D., Hatton, G.B., Wang, J., Buanz, A., Gaisford, S., Basit, A.W., 2015b. Fabrication of controlled-release budesonide tablets via desktop (FDM) 3D printing. *Int. J. Pharm.* 496, 414–420.

Goyanes, A., Det-Amornrat, U., Wang, J., Basit, A.W., Gaisford, S., 2016a. 3D scanning and 3D printing as innovative technologies for fabricating personalized topical drug delivery systems. *J. Control. Release* 234, 41–48.

Goyanes, A., Fernández-Ferreiro, A., Majeed, A., Gomez-Lado, N., Awad, A., Luaces-Rodríguez, A., Gaisford, S., Aguiar, P., Basit, A.W., 2018. PET/CT imaging of 3D printed devices in the gastrointestinal tract of rodents. *Int. J. Pharm.* 536, 158–164.

Goyanes, A., Fina, F., Martorana, A., Sedough, D., Gaisford, S., Basit, A.W., 2017a. Development of modified release 3D printed tablets (printlets) with pharmaceutical excipients using additive manufacturing. *Int. J. Pharm.* 527, 21–30.

Goyanes, A., Kobayashi, M., Martínez-Pacheco, R., Gaisford, S., Basit, A.W., 2016b. Fused-filament 3D printing of drug products: microstructure analysis and drug release characteristics of PVA-based caplets. *Int. J. Pharm.* 514, 290–295.

Goyanes, A., Robles Martinez, P., Buanz, A., Basit, A.W., Gaisford, S., 2015c. Effect of geometry on drug release from 3D printed tablets. *Int. J. Pharm.* 494, 657–663.

Goyanes, A., Scarpa, M., Kamlow, M., Gaisford, S., Basit, A.W., Orlu, M., 2017b. Patient acceptability of 3D printed medicines. *Int. J. Pharm.* 530, 71–78.

Goyanes, A., Wang, J., Buanz, A., Martínez-Pacheco, R., Telford, R., Gaisford, S., Basit, A.W., 2015d. 3D printing of medicines: engineering novel oral devices with unique design and drug release characteristics. *Mol. Pharm.* 12, 4077–4084.

He, Y., Jain, P., Yalkowsky, S., 2010. Handbook of Aqueous Solubility Data, second ed. Taylor and Francis Group.

ICH, 2005. Validation of Analytical Procedures: Text and Methodology. Q2(R1).

Jamrógiewicz, M., 2012. Application of the near-infrared spectroscopy in the pharmaceutical technology. *J. Pharm. Biomed. Anal.* 66, 1–10.

Jérez Rozo, J.I., Zarow, A., Zhou, B., Pinal, R., Iqbal, Z., Romañach, R.J., 2011. Complementary near-infrared and raman chemical imaging of pharmaceutical thin films. *J. Pharm. Sci.* 100, 4888–4895.

Kadry, H., Al-Hilal, T.A., Keshavarz, A., Alam, F., Xu, C., Joy, A., Ahsan, F., 2018. Multi-purposable filaments of HPMC for 3D printing of medications with tailored drug release and timed-absorption. *Int. J. Pharm.* 544, 285–296.

Kempin, W., Franz, C., Koster, L.-C., Schneider, F., Bogdahn, M., Weitschies, W., Seidlitz, A., 2017. Assessment of different polymers and drug loads for fused deposition modeling of drug loaded implants. *Eur. J. Pharm. Biopharm.* 115, 84–93.

Khaled, S.A., Alexander, M.R., Wildman, R.D., Wallace, M.J., Sharpe, S., Yoo, J., Roberts, C.J., 2018. 3D extrusion printing of high drug loading immediate release paracetamol tablets. *Int. J. Pharm.* 538, 223–230.

Khaled, S.A., Burley, J.C., Alexander, M.R., Yang, J., Roberts, C.J., 2015a. 3D printing of five-in-one dose combination poly pill with defined immediate and sustained release profiles. *J. Control. Release* 217, 308–314.

Khaled, S.A., Burley, J.C., Alexander, M.R., Yang, J., Roberts, C.J., 2015b. 3D printing of tablets containing multiple drugs with defined release profiles. *Int. J. Pharm.* 494, 643–650.

Khorasani, M., Edinger, M., Rajjada, D., Botker, J., Aho, J., Rantanen, J., 2016. Near-infrared chemical imaging (NIR-CI) of 3D printed pharmaceuticals. *Int. J. Pharm.* 515, 324–330.

Kollamaram, G., Croker, D.M., Walker, G.M., Goyanes, A., Basit, A.W., Gaisford, S., 2018. Low temperature fused deposition modeling (FDM) 3D printing of thermolabile drugs. *Int. J. Pharm.* 545, 144–152.

Lim, S.H., Kathuria, H., Tan, J.J.Y., Kang, L., 2018. 3D printed drug delivery and testing systems — a passing fad or the future? *Adv. Drug Deliv. Rev.* <https://doi.org/10.1016/j.addr.2018.05.001>.

- 1016/j.addr.2018.05.006.
- Luyptaert, J., Massart, D.L., Vander Heyden, Y., 2007. Near-infrared spectroscopy applications in pharmaceutical analysis. *Talanta* 72, 865–883.
- Maroni, A., Melocchi, A., Parietti, F., Foppoli, A., Zema, L., Gazzaniga, A., 2017. 3D printed multi-compartment capsular devices for two-pulse oral drug delivery. *J. Control. Release* 268, 10–18.
- Martínez, L.M., Videira, M., López-Silva, G.A., De los Reyes, C.A., Cruz-Angeles, J., González, N., 2014. Stabilization of amorphous paracetamol based systems using traditional and novel strategies. *Int. J. Pharm.* 477, 294–305.
- Martínez, P.R., Goyanes, A., Basit, A.W., Gaisford, S., 2017. Fabrication of drug-loaded hydrogels with stereolithographic 3D printing. *Int. J. Pharm.* 532, 313–317.
- Martínez, P.R., Goyanes, A., Basit, A.W., Gaisford, S., 2018. Influence of geometry on the drug release profiles of stereolithographic (SLA) 3D-printed tablets. *AAPS PharmSciTech*. <https://doi.org/10.1208/s12249-018-1075-3>.
- Melocchi, A., Parietti, F., Maroni, A., Foppoli, A., Gazzaniga, A., Zema, L., 2016. Hot-melt extruded filaments based on pharmaceutical grade polymers for 3D printing by fused deposition modeling. *Int. J. Pharm.* 509, 255–263.
- Meza, C.P., Santos, M.A., Románach, R.J., 2006. Quantitation of drug content in a low dosage formulation by transmission near infrared spectroscopy. *AAPS PharmSciTech* 7, E206–E214.
- MHRA, 2018. *British Pharmacopoeia: Appendix XII C – Consistency of Formulated Preparations*, London.
- Muwaftak, Z., Goyanes, A., Clark, V., Basit, A.W., Hilton, S.T., Gaisford, S., 2017. Patient-specific 3D scanned and 3D printed antimicrobial polycaprolactone wound dressings. *Int. J. Pharm.* 527, 161–170.
- Netchacovitch, L., Dumont, E., Cailleaud, J., Thiry, J., De Bleye, C., Sacré, P.Y., Boiret, M., Evrard, B., Hubert, P., Ziemons, E., 2017. Development of an analytical method for crystalline content determination in amorphous solid dispersions produced by hot-melt extrusion using transmission Raman spectroscopy: a feasibility study. *Int. J. Pharm.* 530, 249–255.
- Norman, J., Madurawe, R.D., Moore, C.M.V., Khan, M.A., Khairuzzaman, A., 2017. A new chapter in pharmaceutical manufacturing: 3D-printed drug products. *Adv. Drug Deliv. Rev.* 108, 39–50.
- Ravn, C., Skibsted, E., Bro, R., 2008. Near-infrared chemical imaging (NIR-CI) on pharmaceutical solid dosage forms—Comparing common calibration approaches. *J. Pharm. Biomed. Anal.* 48, 554–561.
- Roggo, Y., Chalou, P., Maurer, L., Lema-Martinez, C., Edmond, A., Jent, N., 2007. A review of near infrared spectroscopy and chemometrics in pharmaceutical technologies. *J. Pharm. Biomed. Anal.* 44, 683–700.
- Sadia, M., Arafat, B., Ahmed, W., Forbes, R.T., Alhnan, M.A., 2018a. Channelled tablets: an innovative approach to accelerating drug release from 3D printed tablets. *J. Control. Release* 269, 355–363.
- Sadia, M., Isreb, A., Abbadi, I., Isreb, M., Aziz, D., Selo, A., Timmins, P., Alhnan, M.A., 2018b. From ‘fixed dose combinations’ to ‘a dynamic dose combiner’: 3D printed bi-layer antihypertensive tablets. *Eur. J. Pharm. Sci.* <https://doi.org/10.1016/j.ejps.2018.07.045>.
- Sadia, M., Sośnicka, A., Arafat, B., Isreb, A., Ahmed, W., Kelarakis, A., Alhnan, M.A., 2016. Adaptation of pharmaceutical excipients to FDM 3D printing for the fabrication of patient-tailored immediate release tablets. *Int. J. Pharm.* 513, 659–668.
- Saeed, M., Saner, S., Oelichmann, J., Keller, H., Betz, G., 2009. Assessment of diffuse transmission mode in near-infrared quantification—Part I: The press effect on low-dose pharmaceutical tablets. *J. Pharm. Sci.* 98, 4877–4886.
- Savitzky, A., Golay, M.J.E., 1964. Smoothing and differentiation of data by simplified least squares procedures. *Anal. Chem.* 36, 1627–1639.
- Scoutaris, N., Viithani, K., Slipper, I., Chowdhry, B., Douroumis, D., 2014. SEM/EDX and confocal Raman microscopy as complementary tools for the characterization of pharmaceutical tablets. *Int. J. Pharm.* 470, 88–98.
- Smith, D.M., Kapoor, Y., Klinzing, G.R., Procopio, A.T., 2018. Pharmaceutical 3D printing: design and qualification of a single step print and fill capsule. *Int. J. Pharm.* 544, 21–30.
- Teixeira, K.S.S., da Cruz Fonseca, S.G., de Moura, L.C.B., de Moura, M.L.R., Borges, M.H.P., Barbosa, E.G., De Lima e Moura, T.F.A., 2018. Use of chemometrics to compare NIR and HPLC for the simultaneous determination of drug levels in fixed-dose combination tablets employed in tuberculosis treatment. *J. Pharm. Biomed. Anal.* 149, 557–563.
- Trafford, A., Jee, R., Moffat, A., Graham, P., 1999. A rapid quantitative assay of intact paracetamol tablets by reflectance near-infrared spectroscopy. *Analyst* 124, 163–167.
- Trenfield, S.J., Awad, A., Goyanes, A., Gaisford, S., Basit, A.W., 2018. 3D printing pharmaceuticals: drug development to frontline care. *Trends Pharmacol. Sci.* 39, 440–451.
- Vakili, H., Nyman, J.O., Genina, N., Preis, M., Sandler, N., 2016. Application of a colorimetric technique in quality control for printed pediatric orodispersible drug delivery systems containing propranolol hydrochloride. *Int. J. Pharm.* 511, 606–618.
- Vakili, H., Wickstrom, H., Desai, D., Preis, M., Sandler, N., 2017. Application of a handheld NIR spectrometer in prediction of drug content in inkjet printed orodispersible formulations containing prednisolone and levothyroxine. *Int. J. Pharm.* 524, 414–423.
- Verstraete, G., Samaro, A., Grymonpré, W., Vanhoorne, V., Van Snick, B., Boone, M.N., Hellemans, T., Van Hoorebeke, L., Remon, J.P., Vervaet, C., 2018. 3D printing of high drug loaded dosage forms using thermoplastic polyurethanes. *Int. J. Pharm.* 536, 318–325.
- Wang, C.C., Tejwani Motwani, M.R., Roach, W.J., Kay, J.L., Yoo, J., Surprenant, H.L., Monkhouse, D.C., Pryor, T.J., 2006. Development of near zero-order release dosage forms using three-dimensional printing (3-DP) technology. *Drug Dev. Ind. Pharm.* 32, 367–376.
- Wang, J., Goyanes, A., Gaisford, S., Basit, A.W., 2016. Stereolithographic (SLA) 3D printing of oral modified-release dosage forms. *Int. J. Pharm.* 503, 207–212.
- Wartewig, S., Neubert, R.H.H., 2005. Pharmaceutical applications of Mid-IR and Raman spectroscopy. *Adv. Drug Deliv. Rev.* 57, 1144–1170.
- Williams, J.M., Adewunmi, A., Schek, R.M., Flanagan, C.L., Krebsbach, P.H., Feinberg, S.E., Hollister, S.J., Das, S., 2005. Bone tissue engineering using polycaprolactone scaffolds fabricated via selective laser sintering. *Biomaterials* 26, 4817–4827.
- Yang, Y., Wang, H., Li, H., Ou, Z., Yang, G., 2018. 3D printed tablets with internal scaffold structure using ethyl cellulose to achieve sustained ibuprofen release. *Eur. J. Pharm. Sci.* 115, 11–18.
- Yu, D.G., Branford-White, C., Ma, Z.H., Zhu, L.M., Li, X.Y., Yang, X.L., 2009a. Novel drug delivery devices for providing linear release profiles fabricated by 3DP. *Int. J. Pharm.* 370, 160–166.
- Yu, D.G., Shen, X.X., Branford-White, C., Zhu, L.M., White, K., Yang, X.L., 2009b. Novel oral fast-disintegrating drug delivery devices with predefined inner structure fabricated by Three-Dimensional Printing. *J. Pharm. Pharmacol.* 61, 323–329.
- Zema, L., Melocchi, A., Maroni, A., Gazzaniga, A., 2017. Three-dimensional printing of medicinal products and the challenge of personalized therapy. *J. Pharm. Sci.*
- Zhang, J., Feng, X., Patil, H., Tiwari, R.V., Repka, M.A., 2017. Coupling 3D printing with hot-melt extrusion to produce controlled-release tablets. *Int. J. Pharm.* 519, 186–197.